LABELING OF TISSUE COMPOSITE WITH FLUORINE NANOEMULSION FOR MAGNETIC RESONANCE IMAGING

by
Shinnosuke Fukazawa

A thesis submitted to Johns Hopkins University in conformity with the requirements for the degree of Master of Science in Biomedical Engineering

Baltimore, Maryland
May 2018

Abstract

The regenerative medicine approach of using stem cells loaded on hydrogel scaffolds has gained wide attention in recent years. Tissue composites made from stem cells embedded in hydrogels provide a minimally invasive strategy for local delivery of stem cells via injection, and simultaneously keep the treatment localized in a controlled environment provided by the scaffold. Such treatment options have been found to be particularly attractive in situations such as joint degeneration, including intervertebral disc disease. A challenge which remains to be addressed with these tissue scaffolds is the ability to image them post-injection into a patient. Imaging of the scaffold provides two major benefits; precision in the deployment of the injected scaffold and insight into the degradation and restructuring of the cellular environment at the treatment site. Herein is described a labeling method which enables imaging of a scaffold under ^{19}F magnetic resonance imaging by the inclusion of a perfluorocarbon nanoemulsion. Tissue composites were developed from thiol-modified hyaluronic acid, perfluorocarbon imaging agent, stem cells, and poly (ethylene glycol) diacrylate was added to cross-link the mixture into a hydrogel. The formulation of the hydrogel was determined based on a possible application in treating intervertebral disc degeneration as it seems well-suited based on recent studies in the field. The utility of the imaging agent was assessed based on viability of the stem cell and the strength of the signal overtime. Bioluminescent signal was measured to determine viability of the stem cells, and ^{19}F magnetic resonance imaging was employed to observe signal strength overtime. Rheology of the hydrogel was used to characterize the physical properties of the hydrogel. Optimal concentration of the imaging agent was studied through the creation of multiple hydrogel scaffolds with varying perfluorocarbon

concentrations. Based on the findings, there is a single optimal level of perfluorocarbon content for tracking a hydrogel tissue scaffold.

Thesis Committee:

Mirosław Janowski

Russell H. Morgan Department of Radiology and Radiological Science, Division of MR Research and Cellular Imaging Section, Institute for Cell Engineering, Johns Hopkins University School of Medicine, Baltimore, MD, USA

NeuroRepair Department, Mossakowski Medical Research Center, Polish Academy of Science, Warsaw, Poland

Piotr Walczak

Russell H. Morgan Department of Radiology and Radiological Science, Division of MR Research and Cellular Imaging Section, Institute for Cell Engineering, Johns Hopkins University School of Medicine, Baltimore, MD, USA

Department of Neurology and Neurosurgery, University of Warmia and Mazury, Olsztyn, Poland

Michael McMahon

Russell H. Morgan Department of Radiology and Radiological Science, Johns Hopkins University School of Medicine, Baltimore, MD, USA

F. M. Kirby Research Center for Functional Brain Imaging, Kennedy Krieger Institute, Johns Hopkins University, Baltimore, MD, USA

Preface/Acknowledgments

First and foremost, I would like to thank my advisor, Miroslaw Janowski, for providing me with an exceptional environment to conduct my research. A mentor caring for his lab members just as much as his research, it was a pleasure working under his guidance.

I would also like to thank Anna Jablonska, a post-doctoral fellow in Dr. Janowski Lab for her daily guidance in my research challenges.

In addition, I would like to thank my parents for their continued support throughout my higher education. They made it possible for me to pursue my dream and career; without them I would have missed this invaluable opportunity.

Finally, I would like to acknowledge my fellow BME Master students. Their companionship has made the 2 years here a wonderful experience.

Table of Contents

List of Figures

1 Background

1.1 Intervertebral Disc Degeneration

A major cause of disability and retirement is lower back pain, which affects more than 630 million globally [1]. The global prevalence for lower back and neck pain is between 22-65%, with an increasing trend [2], [3]. Frequently associated with lower back and neck pain is intervertebral disc (IVD) degeneration.

The IVD is a gel-like material located between vertebrae and makes up roughly 1/4 of the spine. It is made up of two main structures; a tough outer ring known as the annulus fibrosus (AF) and gel-like filling known as the nucleus pulposus (NP). The AF is composed of highly organized type I collagen fibers to form a strong concentric ring. The NP on the other hand has a higher proteoglycan concentration and randomly organized type II collagen fibers. Proteoglycans such as aggrecan and glycosaminoglycans such as chondroitin sulfate found in the NP and are major contributors to the strong water affinity and characteristic compressibility of the IVD. Distinct cell types also regulate the extracellular matrix in each region; chondrocyte-like NP cells in the NP and fibroblast-like AF cells in the AF. Naturally, the IVD degenerates through the combined effects of aging of these cells as well as fragmentation of the proteoglycans and GAGs [4]. With age these regulating cells in the IVD become senescent and decline in number, making it difficult to maintain a proper matrix [5]. Wear and tear also continue to deteriorate the IVD and reduces its resistance to compression and overall disc height [6].

Degeneration of the IVD may lead to other complications. Segmental instability of the spine due to IVD degeneration commonly results in osteophyte formation, which are

bone growths of the vertebrae thought to stabilize a joint through enlargement of the joint surface [7]. Although osteophytes can be helpful by returning lost stability, overgrowth can impinge on the surrounding nerves causing chronic pain. In severe cases of IVD degeneration, the NP may rupture out of the weakened AF, resulting in a significant IVD volume loss. As a result, mobility may be reduced, and the ruptured NP may impinge on the nerves just as the osteophytes can to cause chronic pain.

1.2 Current Techniques for Treatment

IVD degeneration is currently treated in multiple ways on a case-by-case basis. Surgical treatment of IVD degeneration includes discectomy with or without disc replacement and potentially spinal fusion [8]. Spinal fusion involves synthesis of the vertebrae surrounding the problematic disc to stabilize the movement and in theory limit the progression of the disease [9]. Despite short term alleviation of pain, there is a loss of mobility at the involved vertebrae, and there are many reports of adjacent segment degeneration and disease and recurrence of chronic pain [10]. Total disc replacement on the other hand attempts to restore mobility by replacing the damaged IVD with a replacement material. Although some reports show success in the short run, there have been reports of loss of mobility and ankylosis development in the long term as well as adjacent level disc degeneration [11-13]. Nucleus pulposus replacement is a minimally invasive option in which materials such as polymethylmethacrylate and silicon are injected in to NP through the AF. Although minimally invasive, there is concern in the migration of injected materials which tend to be synthetic, gel-like, and degrade mechanically over-

time. Finally, therapeutic options exist such as intradiscal electrothermal therapy, but this is technically not a treatment option but a method to decrease the pain [8].

1.3 Treatment Using Stem Cell Therapy

Previously discussed options are all generally limited in the long-term capability of restoring motion and alleviating chronic pain, and there is a growing consensus for the need of a new therapeutic paradigm. As such, treatment of IVD degeneration through stem cell therapy has received widespread attention in recent years. Stem cell therapy is promising in regards that the stem cells applied for treatment may fully restore the function of the IVD. Since new healthy stem cells are being introduced, they are thought to be capable to proliferate and reconstruct the damaged proteoglycans and glycosaminoglycans, thereby completely restoring IVD to the premorbid status. Mesenchymal stem cells (MSCs) are a type of stem cells which have demonstrated potential to differentiate into multiple types of connective tissues, including those in the NP [14]. In a pilot study on humans, treatments with autologous bone marrow MSCs proved to be effective in improving pain and disability with 71% efficacy, displaying comparably favorable outcome to spinal fusion and total disc replacement [15].

In addition to the potential benefits, stem cell treatments have shown to have some risks. In animal model studies of MSC treatment for IVD degeneration, stem cells were found in some cases to leak out of the NP and differentiate into osteocytes which formed bone spurs [16]. Without proper containment techniques, stem cell injection may instead accelerate disease progression; hence, scaffolds are employed to facilitate localization of MSCs within the intervertebral space. Numerous scaffolds have been investigated such as

alginate, hyaluronan, silk, and many others. Of these scaffold materials, hyaluronan-based hydrogels stand out as a strong stem-cell scaffold candidate for IVD regeneration. These biocompatible hyaluronan-based (HA) hydrogels can be injected in the NP while mitigating the risk of leakage through the AF. Additionally, recent studies have shown that HA hydrogels support differentiation of MSCs into chondrocytes, which are the primary cell type found in cartilage and joints such as IVD [14], [17].

Hyaluronan is a collective term for the physiological forms of hyaluronic acid, a glycosaminoglycan which constitutes the majority of the extracellular matrix [18]. Native and abundant in the human body, hyaluronan is a safe biocompatible material suitable for cell scaffolding. Hyaluronic acid is made by linking D-glucuronic acid and N-acetyl glucosamine together repeatedly. Under physiological conditions it possesses sodium counterions, as hyaluronic acid is strongly negatively charged and hydrophilic. To better control the properties of the scaffold it forms, a number of derivatives have been developed; thiol-modified HA, tyramine-grafted HA, and glycidyl methacrylate-HA are a few that allow in situ cross-linking [19]. Used in conjunction with MSCs, therapeutic effects might be localized in the injection site, and the scaffold matrix adds IVD volume temporarily while the cells contribute to the complete IVD restoration.

1.4 Monitoring the Tissue Scaffold

Imaging of the tissue scaffold is an important possibility to consider for detecting potential leakage from the NP. As aforementioned, cell leakage may lead to osteogenic differentiation of the injected stem cells, which in turn leads to the development of bone spurs that may impinge on the surrounding nerves. By imaging the scaffold during its

injection, precise localization can be ensured which are then monitored over time for leaks. An additional benefit is the capability of monitoring scaffold degradation. It is generally considered that the scaffold should gradually degrade as the tissue regenerates in order to support growth without limiting space for further development [20]. By making the scaffold imageable, progress of NP regeneration can be indirectly gauged non-invasively.

Several methods of imaging have been explored as options to image hydrogels in situ. Some imaging modalities include the inclusion of image contrast agent within the hydrogels such as iodine and gold for X-Ray/computed tomography (CT), gadolinium for magnetic resonance imaging (MRI), and various fluorescent markers for fluorescence confocal microscopy [21]. Alternatively, certain imaging methods developed exploit properties of the hydrogels to obtain endogenous signal, such as Raman-based imaging of alginate and chemical exchange saturation effect MRI (CEST MRI) of gelatin [22], [23]. In this thesis another modality is described which is the use of perfluorocarbon nanoemulsion for ^{19}F MRI.

1.5 Overview of ^{19}F MRI

^{19}F MRI is a technique which employs the detection of resonances produced by ^{19}F nuclei in a magnetic field to create images. The NMR detectable ^{19}F nucleus has 100% natural abundance, and possess a gyromagnetic ratio which is the highest besides ^{1}H; this results in high MRI sensitivity and allows its use for a variety of MR applications. Unlike the ^{1}H nucleus, which is the typical source of signal for MRI, there is a low level of naturally available ^{19}F in the human body. As such, ^{19}F MRI allows for imaging of exogenous imaging agents without any background present, resulting in “hot spots” where

agents are located. The signal may be conveniently mapped by overlaying ^{19}F signals onto ^{1}H images. Additionally, because the gyromagnetic ratio of ^{19}F, 40.08MHz/T, is very similar to ^{1}H, 42.58MHz/T it is possible to produce coils capable of detecting both nuclei either by retuning between scans or having double resonance circuits. Other nuclei will be more complicated to use for hot spot imaging due to sensitivity challenges or requirements for hyperpolarization equipment [24]. An additional benefit of having similar NMR characteristics is that most sequences used in ^{1}H have been adapted to ^{19}F and will use the same transmit and receive hardware on the scanners. Fast imaging methods used in ^{1}H scans such as fast low angle shot (FLASH), fast low angle rapid acquisition with relaxation enhancement (FLARE), rapid acquisition with relaxation enhancement (RARE) all exist for ^{19}F and can easily be applied with only slight modifications to the original pulse sequences [25], [26].

Currently, ^{19}F MRI finds itself used in a variety of applications including inflammation imaging, stem cell tracking, lung imaging, and monitoring of drug-delivery [27]–[30]. Cell tracking is possible through the cellular absorption of highly inert fluorine nanoemulsions while lung imaging employs inert fluorinated gases and monitoring of drug delivery employs nanocarriers which include fluorine in their formulation. Cell tracking is particularly challenged by the limited amount of ^{19}F which can be taken up by cells, resulting in relatively low detection sensitivity. In contrast to direct internalization of fluorine by cells, hydrogels can be labelled with much higher quantities of fluorine, which increases their detectability by MRI. Here a nanoemulsion, which is made by emulsifying perfluorocarbons, was integrated into the hydrogels to provide an exogenous signal to map the tissue composite. Other methods which directly fluorinate the cell scaffold have been

attempted previously, for example fluorination of polyurethane was performed by Lammers et al. [31]. The method here is simpler, and the result is sharp ^{19}F resonance which can be readily and sensitively detected.

Use of ^{19}F imaging agents can sometimes be advantageous compared to ^{1}H contrast agents based on gadolinium, manganese, or super paramagnetic iron oxides which reduce local $^{1}H_2O$ (water) relaxation times and thereby alter the water signal. Signal changes produced by these contrast agents are sometimes challenging to differentiate from changes produced by biological events such as infection, hemorrhage or other sources, which can be problematic [32]. Obtaining favorable MR images also generally requires large amounts of contrast agent due to low polarization of $^{1}H_2O$ in a magnetic field, and injections of large volume of heavy metals such as gadolinium may lead to adverse events such as Nephrogenic Systemic Fibrosis [33]. Perfluorocarbons are well tolerated at high doses and have been used as blood substitutes [34].

Despite these advantages, ^{19}F MRI still has limitations to overcome. The main problem with ^{19}F MRI is the much lower spatial resolution compared to that of a ^{1}H scan. This is largely due to the relatively low quantity of fluorine injected compared to the ~110 M water in biological tissue, which results in a diminished signal to noise ratio (SNR) compared to a ^{1}H scan [35]. The reception of the ^{19}F detection coil is also a factor. Due to this, single-frequency-mode RF coils are often used to maximize SNR, which requires coil swapping or retuning. Additional time for imaging is thus required, and the extra motion can also affect the co-registration process of mapping the ^{19}F to the ^{1}H scan. Auto-tuning RF coils and dual-mode RF coils exist, but they are not particularly prevalent, particularly in the clinical setting, due to the increased complexity and cost required. Some of these

problems are currently being addressed though, such as the development of cryogenic RF coils with high SNR by a research group in Charité University [36]. With the advancement of ^{19}F MRI technology and the presence of a wide variety of fluorine drugs and applications, ^{19}F MRI technique remains promising with respect to clinical applications in the near future.

2 Experimental Methods for Fluorine Hydrogel

2.1 Materials

To assess the efficacy of perfluorocarbon as an imaging agent, the rheological effect on hydrogels, viability of the cells co-residing in the hydrogels, and the capability to image over-time were measured. The perfluorocarbon nanoemulsion used was VS-1000H (Celsense, Inc., PA 15222), a pre-clinical grade emulsion of perfluoro crown ether in clinical grade water for injection. The scaffold material was constructed using thiol-modified hyaluronan (Glycosil®, ESIBIO, Alameda, CA 94501) and a thiol-reactive PEGDA crosslinker (Extralink®, ESIBIO) that has a molecular weight of 3400 Da. Both the thiol-modified hyaluronan and the thiol-reactive cross-linker were desiccated with PBS salts such that when reconstituted according to the manufacturer's protocols, they were 1% wt./vol. in 1x PBS. The structures of the hyaluronan and PEGDA can be seen in Figure 1 and Figure 2. The PEGDA is used to cross- link the thiol-modified hyaluronan, although it is noted that the hyaluronan can cross-link between itself at a much slower rate in the presence of air.

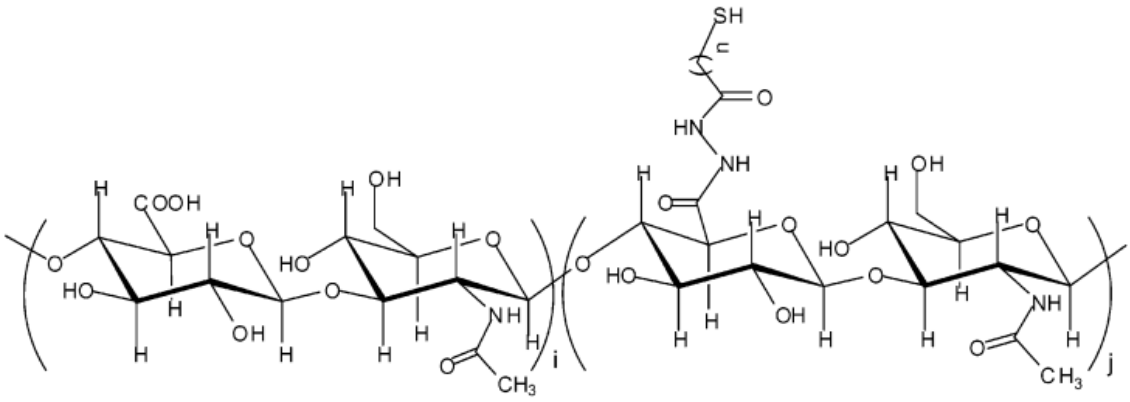

Figure 1: Structure of thiol-modified hyaluronan. The thiol-modification is depicted as a hanging structure on the top of the figure. Thiolation of hyaluronan allows hyaluronan, which otherwise cannot gelate, to form a hydrogel.

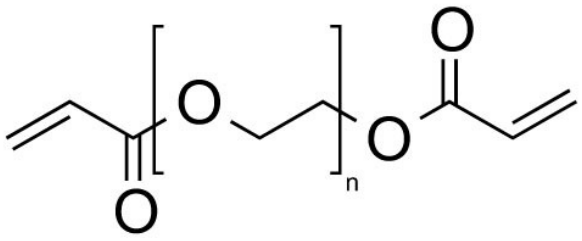

Figure 2: Structure of Poly (ethylene glycol) diacrylate or PEGDA. PEGDA is important in cross-linking of the thiol-modified hyaluronan into a hydrogel.

2.2 Cell Culture

Stem cells used in the tissue scaffold were mesenchymal stem cells (MSCs) with luciferase expression which were derived from the bone marrow of luciferase expressing transgenic FVB mice. To obtain the stem cells, the femurs and tibia were removed from the mice, and cells were flushed out using a needle and 1x PBS. All cells flushed out were then collected and centrifuged. The resulting cell pellet was reconstituted using culture media and seeded in a T-75 polystyrene flask. The culture media used was composed of Dulbecco's Modified Eagle's Medium (Gibco®), 10 % volume of fetal bovine serum (Gibco®), 1% volume of antibiotics (10,000U/mL penicillin and 10mg/mL streptomycin).

Hematopoietic cells and other non-MSCs were removed through selective culturing, and after the second round of passaging the phenotype in the flask was observed to be homogenous.

2.3 Hydrogel Preparation

Hydrogels were formed with the following components: thiol-modified hyaluronic acid (HA), PEGDA, VS-1000H (VS), and MSCs. 4 different concentrations of VS were tested to study its impact on the gels. First the HA and PEGDA were reconstituted accordingly to the manufacturer's protocol from its powder form to 1% wt./vol using degassed water. VS was subsequently added at varying ratios to HA creating 4 groups: 1:0 HA:VS (no VS), 50:1, 10:1, 5:1, and 1:1. MSCs were detached from the cell culture flask through trypsinization and centrifuged. The cells were then resuspended to a concentration of $2x10^7$ cells/mL in cell culture media and added to the hydrogel mixture to make up 7.4% of the final hydrogel volume which equates to ~1.5 million MSC/mL of hydrogel. Cross-linking was then initiated by adding PEGDA at a ratio of 4 HA to 1 PEGDA by volume. The mixture was then pipetted carefully until a homogenous hydrogel was formed. The 1:1 hydrogel did not form a stable hydrogel due to the lowered concentration of HA; therefore, this hydrogel formulation is not discussed henceforth.

2.4 Rheology

A rheological study of the hydrogels was performed to obtain the stiffness (storage modulus) and the gelation kinetic of the hydrogels. Measurements were made on an ARES-G2 rotational rheometer (TA Instruments, New Castle, DE 19720). The gelation kinetics

for the hydrogel was studied using a 25mm flat plate geometry, and the environment was set to 37°C with controlled humidity using Peltier solvent trap and evaporation blocker. The storage modulus was measured for 1 hour using a step time of 8s at a rotational frequency of 1Hz with an oscillation strain of 1±0.02%. Measurements were recorded promptly after mixing the proper ratios of hyaluronan, PEGDA, and VS-1000H.

2.5 Cell Viability

In Vitro

The viability of MSCs was determined for each type of hydrogels. Preparation of the hydrogels was done by mixing the contents in a 1.5mL conical Eppendorf tube using a pipette. Each type of hydrogel was then seeded as triplicates of 50μL volume onto a flat bottom 96-well plate for a grand total of 12 wells. The viability was measured through bioluminescent signals of the MSCs using Victor^3 Multilabel Microplate Reader (PerkinElmer). Prior to imaging, a stock 30mg/ml D-luciferin (D-Luciferin, Potassium Salt, GOLD BIOTECHNOLOGY, Inc., St. Louis, MO) solution in PBS was mixed with cell culture media to create 0.2mg/mL dilution. Media from the cell culture plate was aspirated carefully and replaced with 100μL of 0.2mg/mL D-luciferin solution using a multi-channel pipette. The plate reader was set to 37°C, and each well was imaged with 3s exposure and measurement of the plate repeated until a peak signal was observed.

In Vivo

The viability of the MSCs injected within the scaffold was observed in mice. Prior to hydrogel injection, the mice were prepared for injection and bioluminescent imaging by

shaving and application of Nair for complete hair removal on the back. Preparation of the hydrogel was done through a mixture of the contents in a 1.5mL conical Eppendorf tube. As the gelation time approached, the hydrogel was loaded on to a 27-gauge 1mL syringe. The hydrogel was injected in 50μL volumes subcutaneously on the dorsal side along the left and right sides of the spine. Injections were done in triplicates where each group of the same hydrogel was injected columnar down the spine, totaling 6 injections per mice. The mice used were RAG2 KO (B6(Cg)-*Rag2*$^{tm1.1Cgn}$/J, The Jackson Laboratory) and were 3 months old.

Prior to imaging, 150μL of 30mg/ml D-luciferin solution in PBS was injected into each mouse intraperitoneally. The mice were then put under gas anesthesia with 2.5% isoflurane and imaged for bioluminescence using IVIS Spectrum (PerkinElmer) optical imaging device after 1 day and then weekly.

2.6 ^{19}F MR Imaging

In Vitro

Imaging of hydrogel phantoms with perfluorocarbon agent was studied. First, 100μL volume hydrogels were formed in 0.5mL conical polypropylene tube with the same formulation as aforementioned in section 2.3, but without the addition of the cell suspension. Two of each hydrogel types containing VS was created and one hydrogel without VS. 100μL of 1xPBS was added above the formed hydrogel to prevent its dehydration. The PBS was replaced every other day as a parallel to the in vitro viability study where the cell culture media was replaced every other day.

Imaging was performed on a vertical bore 17.6T scanner (Bruker Avance 750 WB), using a $^{1}H/^{19}F$ dual-mode volume coil. ^{1}H images were acquired at 750MHz and ^{19}F images at 705.5MHz. ^{1}H images were acquired using rapid acquisition with relaxation enhancement (RARE) sequence with the following parameters: echo time (TE) = 6.260ms, Rare Factor = 8, Repetition Time = 2500.000ms, Number of Average (NA) = 1, Spatial Resolution = 0.1953125mm x 0.1953125mm, FOV = 25mm x 25mm. ^{19}F image were acquired with a modified RARE sequence with the following parameters: TE = 5.79ms, Rare Factor = 8, Repetition Time = 1000ms, NA = 32, Spatial Resolution = 0.78125mm x 0.78125mm, FOV = 25mm x 25mm. The phantoms were imaged for 12 weeks. A reference glass capillary tube with VS was included to use as a reference for intensity comparison. The intensity measurement overtime was analyzed using the software Voxel Tracker 2.0 (Celsense, Inc.).

In Vivo

The same mice from the cell viability study was used for ^{19}F MRI. Mice were sedated using ketamine/xylazine cocktail (100mg/kg, 10mg/kg), and subsequently imaged using the same coil and imaging parameters as the *in vitro* study. A reference glass capillary tube containing VS was placed on the ventral side of the mice. Signal intensity of the images were analyzed using Voxel Tracker 2.0 to make a comparison.

3 Experimental Results

3.1 Rheology

The storage modulus of all hydrogel formulations is presented in Figure 3. From the figure it is evident that the gelation is delayed by the addition of VS to the hydrogel. Additionally, the plateau of the exponential increase in storage modulus is lower as the VS concentration increases, showing that VS plays a role in lowering the overall storage modulus or stiffness of the hydrogel. The results also indicate that the 50:1 addition of VS is too low of a concentration to affect the rheology of the hydrogel.

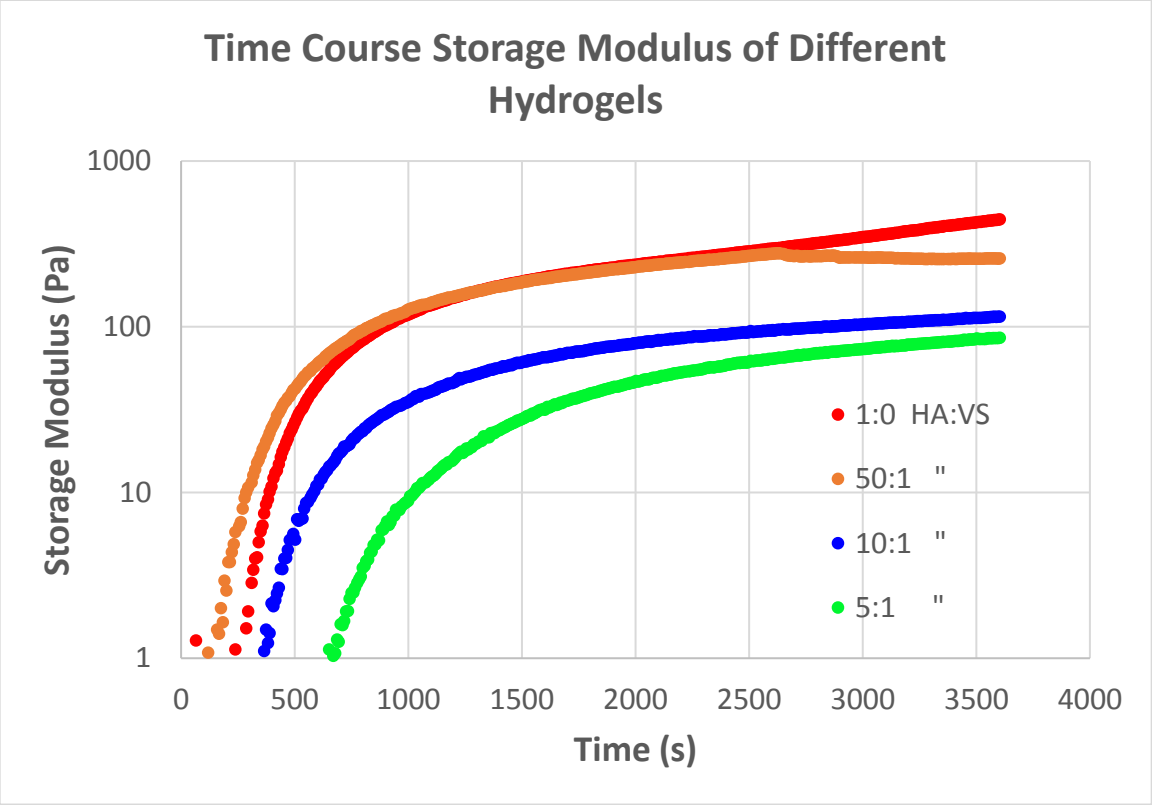

Figure 3: Rheometric measurement of the in situ hybridization of hyaluronan hydrogels using ARES-G2 rotational rheometer. Storage modulus of the hydrogel as it gelates is plotted against time. The points shown are in step time of 8s, and some negative readings were omitted in the logarithmic depiction of the data.

3.2 Cell Viability

In Vitro

The longitudinal BLI study of the in vitro experiment is shown in Figure 4. Initially, there was a strong variability in the BLI signals between the hydrogel samples with 5:1 hydrogel having a much stronger signal compared to the other hydrogels. On day 3, there was a sharp attenuation in signal strength and followed by another period of strong signal on day 7. This trend of fluctuation continued until the fluctuation seemed to damp out around week 6, and by week 8 the signal strength from strongest to weakest was consistently 5:1, 10:1, 50:1, and 1:0. This indicates that VS has a positive effect on the viability of the hydrogels.

The bar for 1:0 in Figure 4 shows that out of the triplicates measured, one of the wells consistently had baseline level signals. This indicates that the cells in this well was not viable from the start although the reason is not clear. The graph seems to indicate that the 1:0 hydrogel would have had comparable signal to that of the 50:1 gel up until day 35, at which point the signal fluctuation seemed to dampen as the other hydrogel types, albeit at a lower final signal strength.

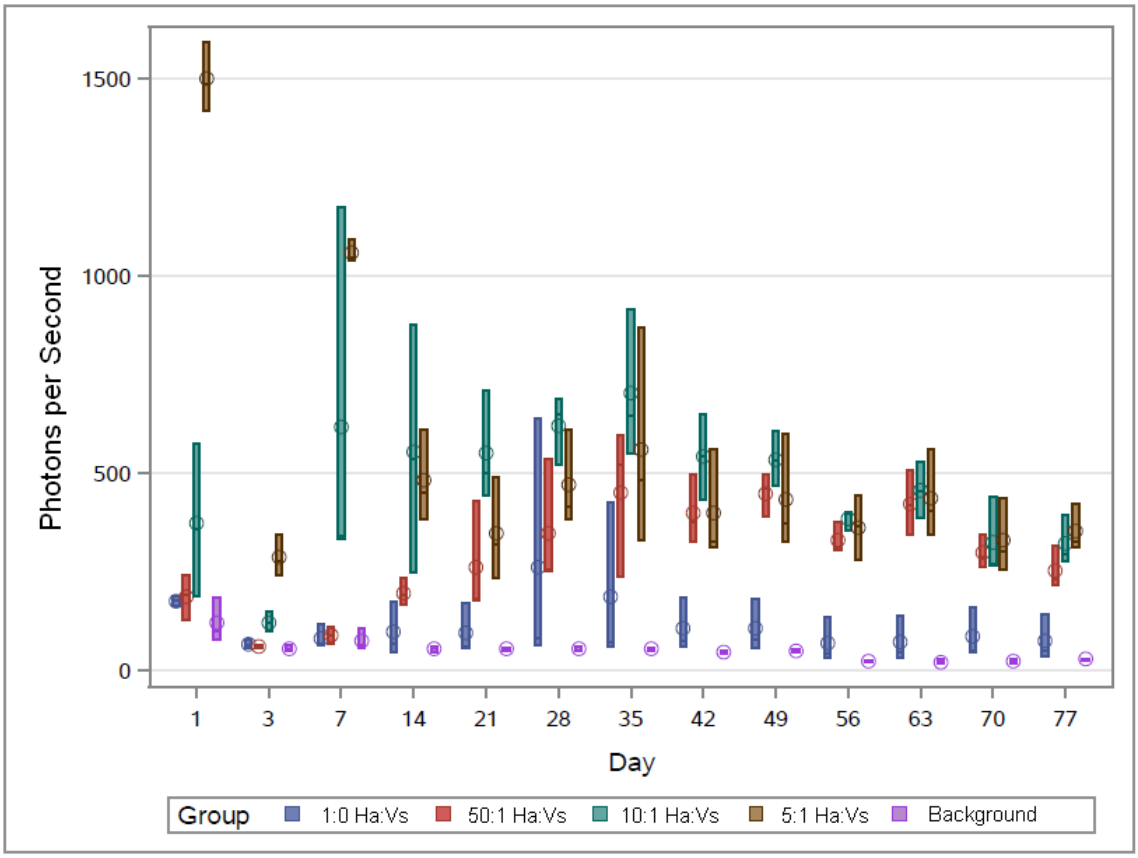

Figure 4: Overtime BLI measurements of tissue scaffold in vitro. The 96 well-plate containing MSCs in hydrogel was imaged for 11 weeks.

In Vivo

A sample BLI measurement of mice can be seen in Figure 5. The heat map of the BLI signal was generated using Living Image software. Equal sized region of interests

(ROIs) were selected on the heat map over the 12 injections, and the signal strength overtime is plotted in Figure 6. Initial signal was strongest for the 10:1 gel, followed by the 5:1 gel, and lowest signal between 1:0 and 50:1. The similarity of the 50:1 to the 1:0 suggests that the low level of V-sense is not enough to contribute any noticeable effects to the cell viability. Viability decreased for all gels over the course of 4 weeks but at the last week, there were signs of signal recovery in the 10:1 gel suggesting some proliferation and remaining viable cells. There is also a similar trend here as the in vitro measurements where there is a high initial standard deviation for higher VS concentration gels. VS seems to add an element of unpredictability to cell viability; however, in all cases it is seen that the deviations between the samples decline overtime, mainly due to the decline in overall signal. Here we determined that the 10:1 gel is most promising for injection based on the initial and final signal level obtained.

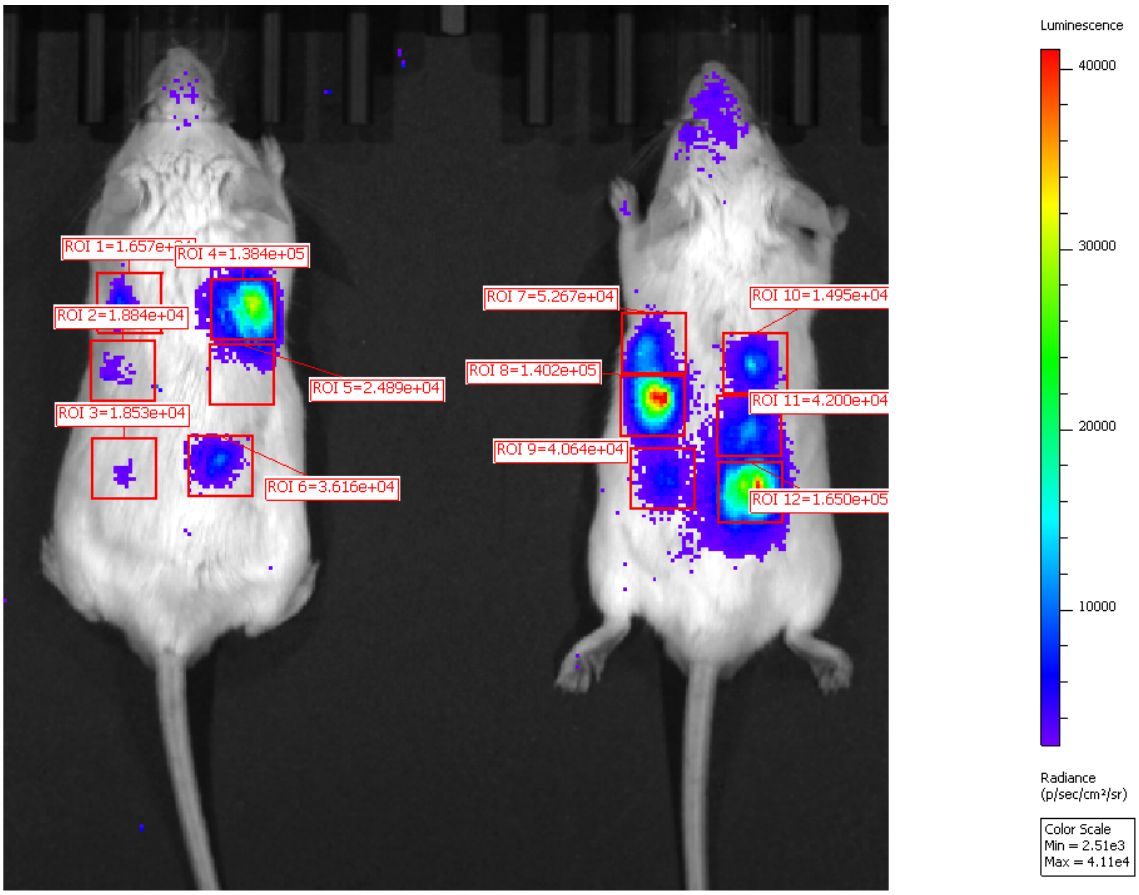

Figure 5: BLI signal heatmap generated using Living Image software. The measurement is from 3 weeks post injection of the tissue scaffold. Variability in the heatmap can be seen between the injection sites, but they are generally on the same order within each column of injection.

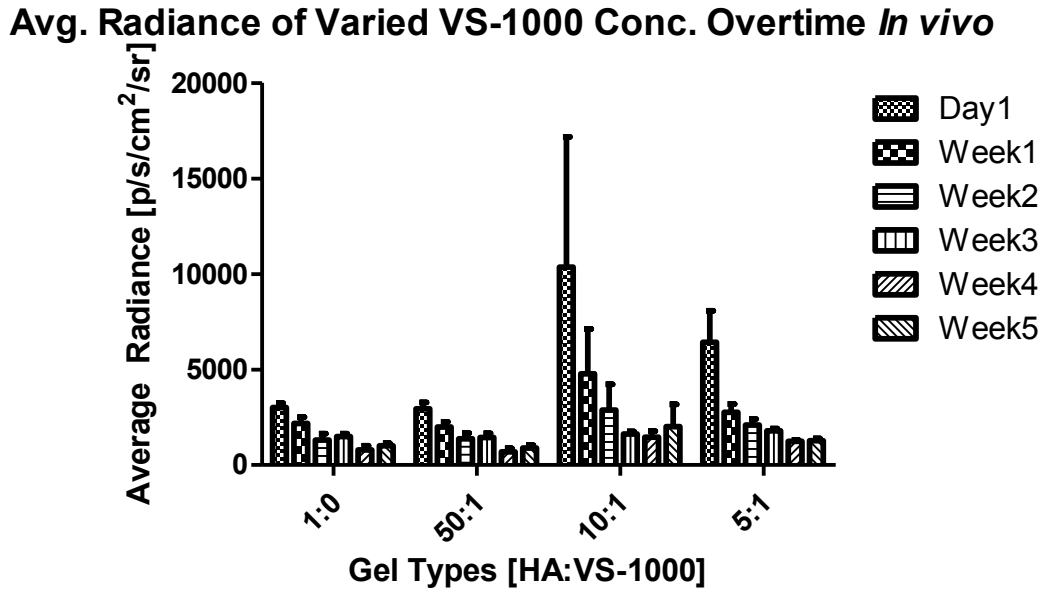

Figure 6: Overtime in vivo measurements of BLI signal from injected MSCs in hydrogel. ROI from the BLI image was analyzed weekly and plotted. The data represents the mean of 3 injections per gel type and the signal intensity is measured by the average radiance within the ROI.

3.3 ^{19}F MR Imaging

In Vitro

Measurements of the phantoms were performed overtime on a weekly basis to track the signal strength of fluorine. Typical MRI images produced can be seen in Figure 7. The image was processed using ImageJ; ^{19}F signal is represented using color map hot, ^{1}H signal is represented using grayscale, and low-signal noise was filtered. The signal strength is as expected with the highest VS concentration (5:1) phantom having the strongest signal intensity followed by 10:1 then 50:1. The control phantom here is the 1:0 hydrogel which contains no fluorine and thus has no observable ^{19}F signal. The reference placed along the phantom is pure VS in capillary used to interpolate the intensity of the phantoms over time. The longitudinal signal intensity change can be seen in Figure 8. The signal intensity in units of procedure defined unit (p.d.u.) is shown in the graph. To make qualitative

measurements, the reference signal was used to assign values to the signal intensity of the hydrogel phantom. From the figure it is evident that after 1 week from the hydrogel creation, the 10:1 and 50:1 hydrogels retained their fluorine content well. On the other hand, the 5:1 hydrogel lost signal overtime suggesting that the lowered concentration of hyaluronan relative to VS allowed VS to escape out of the scaffold. Again, the 10:1 formulation seems to be the best as it maintains strong signal without sacrificing much of its imaging stability as the 5:1 hydrogel did.

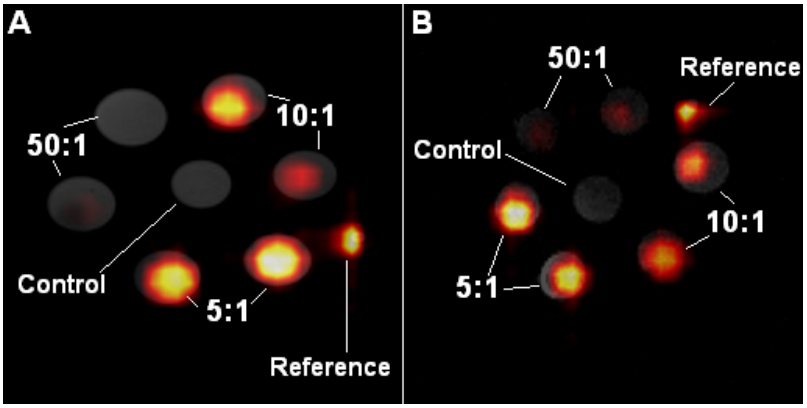

Figure 7: ^{19}F image overlay (shown in red) on ^{1}H image (shown in grayscale). A) Day 1 after phantom creation, B) 10 weeks after phantom creation. The reference location changed slightly over each imaging session, but the reference and its fluorine content remained the same.

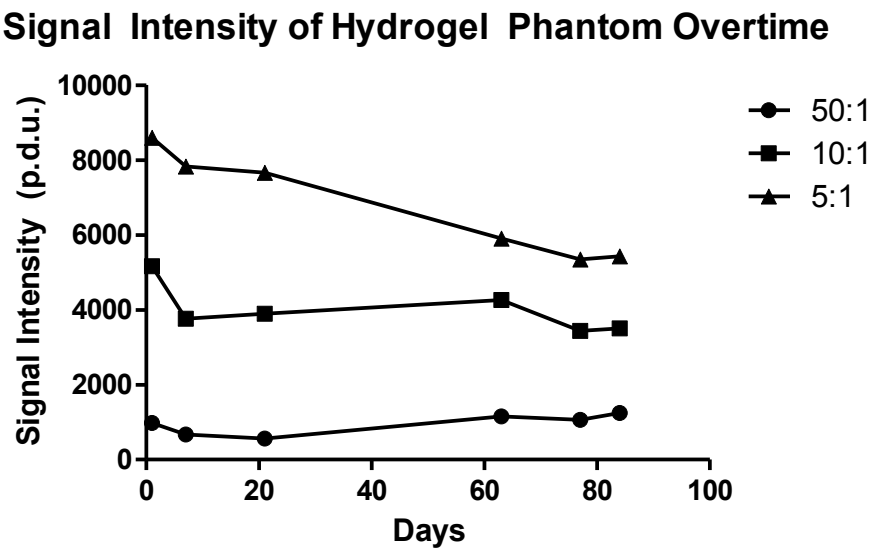

Figure 8: Plot of the signal intensity of hydrogel phantoms measured overtime. Signal intensity was measured in procedure defined units measured from the relative intensity to a reference signal. The calculations were performed on Voxel Tracker 2.0. After an initial signal decrease from Day 1 to Day 7 signal strength was relatively constant for the 10:1 and 50:1 hydrogel. The 5:1 hydrogel had a continuous drop in signal, although even after 12 weeks the signal remained stronger than the 10:1 hydrogel.

In Vivo

$^{1}H/^{19}F$ T2-weighted images of mice were acquired using RARE sequence. A typical image obtained from the process can be seen in Figure 9. 5:1 and 10:1 hydrogels emit a strong signal which can be clearly visualized, while the 50:1 remains difficult to detect. In certain time points, 50:1 hydrogels did not produce strong enough signal to be detectable post-processing for low signal-noise removal. Signal strength overtime is shown in Figure 10. Based on the graph it is clear that the 50:1 formulation does not contain adequate levels of fluorine for imaging. The signal was below background levels and not detectable on weeks 2 and 8. As for the 5:1 and 10:1 hydrogels, their signal was continuously detectable. Due to the susceptibility of the signal to noise and changes in coil receptivity, it is difficult to make absolute statements about what is the minimum detectable threshold; however, the

week 3 image contained one of the weakest signal for the 10:1 hydrogel but as seen in Figure 9, the 10:1 signal is clearly visible.

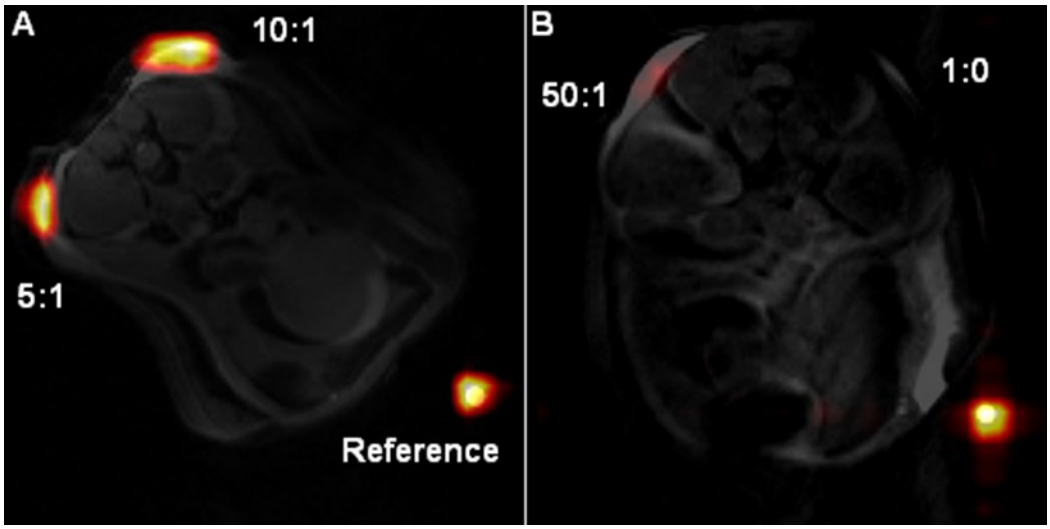

Figure 9: MRI image of a mouse 2weeks post-injection. Cross-section of the mice are shown to visualize the origin of the ^{19}F signal. It is evident from the image that the reference signal is displayed with equal intensity in both images, allowing for a visual comparison of the two. The 50:1 signal is much weaker than the 5:1 and 10:1 signals, and the 1:0 is not detectable with ^{19}F MRI as expected.

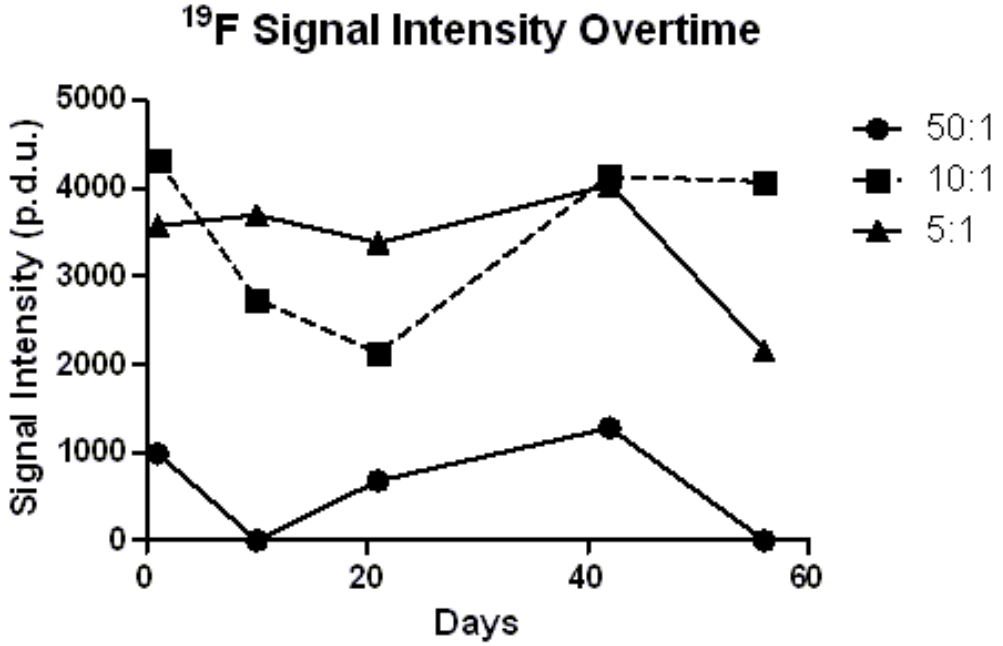

Figure 10: Signal intensity of injected tissue scaffolds overtime. Intensity is in procedure defined unit calculated based on the signal intensity relative to the reference signal in the MR image. Week 2 and week 8 imaging failed to detect any significant signal from the 50:1 phantom.

4 Discussion

The results obtained show that the use of perfluorocarbon nanoemulsions is a promising image labeling strategy for tissue composites. We have found only one study of ^{19}F injectable tissue composite labeling, and one long-term cytotoxicity study of a clinically non-relevant method of imaging using fluorescent quantum dots used in silk-based scaffold, but the imaging tracer was found to lose signal nearly 10 times the rate found here and proved to be cytotoxic [37].

Other groups using a poly(L-glutamic acid)-graft- tyramine/poly(ethylene glycol) hydrogel, which have similar rheological characteristics to the hyaluronan hydrogel here, found that cell viability was increased for hydrogels loaded with increased amount of therapeutics [38]. The authors suggested that increased gaps in the cross-linked network of the hydrogel may produce this effect, which seems similar to the results found here, where increased VS led to better viability. Other methods which attempted MRI tracking through cell-based labelling rather than labeling the hydrogels itself found that there is signal intensity dilution as the cells proliferated and migrated [39]. Although this is not necessarily a negative feature, the application to IVD regeneration may be limited due to the sparse cell placement in the IVD and the requirement to monitor for leakage would likely need a higher concentration of image contrast agent which is easier done by incorporating into the scaffold instead of cells. Still there are many other options, such as chemical immobilization of the imaging agent to the scaffold, where incorporation of such techniques may prove valuable in developing a better tissue composite [40].

4.1 Limitations

The rheological measurements made during the *in situ* hybridization clearly show that VS plays a role in lowering the stiffness of the hydrogel. From the BLI measurements it is also evident that VS enhances cell viability. It is thus difficult to attribute what exact property(ies) of VS contributes to the enhanced cell viability, but there are some theories to explain this phenomenon. One possibility is that the cell viability is affected by the storage modulus of the hydrogel it is in. The hydrogel storage modulus is correlated to the degree of cross-linking between the hyaluronan, and as the storage modulus decreases the diffusion of nutrients to the cells maybe enhanced. The lowered cross-linking may also provide more space for cell proliferation and development of its own extracellular matrix which would lead to better cell survival overtime. Another possibility is due to the gas dissolving properties of VS, or perfluorocarbons in general. Perfluorocarbons have a high gas solubility due to the weak intermolecular forces between themselves, and some perfluorocarbons such as perfluoromethylcyclohexane can have over 300 times the solubility of nitrogen gas compared to water [41]. The increase in gas solubility would allow oxygen to be more readily available to nearby cells which would also keep them viable for longer periods. The oxygen may also play a role in speeding up the bioluminescence reaction. Equations (1) and (2) show part of the light emitting reaction of luciferin, and it shows that oxygen is required to produce light [42]:

$$luciferin + ATP + Enzyme \xrightarrow{Mg^{2+}} Enzyme\ bound\ luciferyl\ adenylate + Phosphate \ldots (1)$$

$$Enzyme\ bound\ luciferyl\ adenylate + O_2 \rightarrow dehydrolufciferin + Enzyme + CO_2 + AMP + light \ldots (2)$$

By providing more oxygen, ATP production for step 1 and conversion of enzyme-bound luciferyl adenylate may occur at a more rapid pace leading to increased bioluminescence

in a given time frame. In such a manner, VS may provide the capability to increase bioluminescence which was interpreted as a higher viability in the hydrogel.

In the *in vivo* MRI, a fluctuation in signal intensity was detected. After the experiments were conducted, it was later determined that the primary cause of the fluctuation was due to the change in the reference signal. In the vertical bore of the MRI, the VS in the reference capillary tube slowly separated with the dense perfluorocarbon nanoemulsions slowly settling. This occurred partly due to the degradation of VS emulsions over time, allowing the perfluorocarbons to settle to the bottom. The differences in reference concentration overtime caused a false drop in signal for the week 2 and week 3 measurements as the condensed reference and the implanted hydrogels were compared. Post week 3 this was accounted for and a fresh set of stable VS was used for each round of measurement. A lesser cause of these fluctuations was due to inevitable systematic errors between imaging sessions. Mice were not imaged at exactly the same location every single time leading to minor differences in read out. This problem was mitigated by the usage of a thin slice geometry to sample the cross section of the mice at a higher geometric frequency.

Despite the *in vivo* MRI having issues of calibration, the *in vitro* results seem to be in a stable condition. Despite the steady decrease in signal intensity of the 5:1 hydrogel, it is evident that the rest of the hydrogels do not follow this trend. In fact, the signal increases, were likely due to hydrogel shrinkage or unavoidable systematic errors in the imaging such as field homogeneity, variations in tuning, and many other possible causes. As the signal slightly increases in the other two, the drop of signal in the 5:1 cannot be attributed to sedimentation of the VS emulsions in the reference capillary. Additionally, the imaging of

the *in vitro* phantoms was conducted before the *in vivo* measurements, and thus likely that the VS was in a more stable condition.

To clarify the cause of enhanced cell viability when VS is added to the hydrogel scaffold, more tests need to be performed. A production of hydrogel diluted simply with clinical water for injection, which the perfluorocarbon was suspended in, in the same ratio as the VS (1:0, 50:1, 10:1, and 5:1) would allow to see if dilution of hyaluronan was a key factor in improving cell viability. If the lowered hyaluronan concentration is indeed the contributing factor to improvement of cell viability, a comparison can be made to see if the VS emulsion has different effects on cell viability compared to water. Next, to test if VS speeds up bioluminescence to produce an erroneously high cell viability measurement, VS can be added to the luciferin solution to see whether the bioluminescence signal shows up brighter and achieves a peak signal earlier. Determining the validity of bioluminescence when measured in the presence of VS means cell viability will not be required to be tested in an alternative method.

If BLI measurements are invalid, another form of viability test which avoids the use of metabolic activity would be preferred such as a DNA/nuclei binding fluorescent marker. Such markers will allow viability tests independent from the oxygen level in the hydrogel. Such viability tests were not optimal for an overtime experiment conducted here, as the fluorescent markers generally have a very specific incubation time assuming it is in direct contact with the cells; in hydrogels, the fluorescent markers must be diffused in through the hydrogels and into the cells then subsequently washed out of the hydrogel scaffold for an accurate reading which is impossible. Measuring in this method, will therefore require the use of a detergent such as hyaluronidase to digest the hyaluronan

scaffold and to subsequently collect the cells through centrifugation to tag with fluorescent markers. Secondly, in vivo measurements would be orders of magnitude more difficult provided that the implanted hydrogels much be excised and the native tissue/cells somehow removed before the digestion of the scaffold.

4.2 Conclusions

Hydrogels with physically immobilized perfluorocarbon allows imaging of the injected tissue composite for a long time. As these particles were not found cytotoxic either, tissue composites with these particles embedded may be functional in clinical application. Next steps to take would require a study of the differentiation of MSCs cultured into these scaffolds. Checking if perfluorocarbon inhibits chondrogenic differentiation or promotes some other differentiation pathway should be studied in order to ensure its proper application. Effects of differences in 3D culture conditions also remain to be studied; the differences in culturing a thin sheet of tissue composites on a well-plate against a much larger volume similar to what would be used clinically may provide significant differences in viability of the cells.

5 References

[1] T. Vos *et al.*, "Years lived with disability (YLDs) for 1160 sequelae of 289 diseases and injuries 1990–2010: a systematic analysis for the Global Burden of Disease Study 2010," *The Lancet*, vol. 380, no. 9859, pp. 2163–2196, Dec. 2012.

[2] Hoy Damian *et al.*, "A systematic review of the global prevalence of low back pain," *Arthritis Rheum.*, vol. 64, no. 6, pp. 2028–2037, May 2012.

[3] B. I. Martin *et al.*, "Expenditures and Health Status Among Adults With Back and Neck Problems," *JAMA*, vol. 299, no. 6, pp. 656–664, Feb. 2008.

[4] P. J. Roughley, "Biology of Intervertebral Disc Aging and Degeneration: Involvement of the Extracellular Matrix," *Spine*, vol. 29, no. 23, pp. 2691–2699, Dec. 2004.

[5] S. Roberts, E. H. Evans, D. Kletsas, D. C. Jaffray, and S. M. Eisenstein, "Senescence in human intervertebral discs," *Eur. Spine J.*, vol. 15, no. 3, pp. 312–316, Aug. 2006.

[6] R. Sztrolovics, M. Alini, P. J. Roughley, and J. S. Mort, "Aggrecan degradation in human intervertebral disc and articular cartilage.," *Biochem. J.*, vol. 326, no. Pt 1, pp. 235–241, Aug. 1997.

[7] A. Fujiwara *et al.*, "The effect of disc degeneration and facet joint osteoarthritis on the segmental flexibility of the lumbar spine," *Spine*, vol. 25, no. 23, pp. 3036–3044, Dec. 2000.

[8] Département de l'Appareil Locomoteur, Site Hôpital Orthopédique, Centre Hospitalier Universitaire Vaudois and The University of Lausanne, Avenue Pierre-Decker 4, CH-1011 Lausanne, Switzerland, C. Schizas, G. Kulik, and V. Kosmopoulos, "Disc degeneration: current surgical options," *Eur. Cell. Mater.*, vol. 20, pp. 306–315, Oct. 2010.

[9] T. J. Kishen and A. D. Diwan, “Fusion Versus Disk Replacement for Degenerative Conditions of the Lumbar and Cervical Spine: Quid Est Testimonium?,” *Orthop. Clin. North Am.*, vol. 41, no. 2, pp. 167–181, Apr. 2010.

[10] J. S. Harrop *et al.*, “Lumbar Adjacent Segment Degeneration and Disease After Arthrodesis and Total Disc Arthroplasty,” *Spine*, vol. 33, no. 15, pp. 1701–1707, Jul. 2008.

[11] J. E. Zigler, “Clinical results with ProDisc: European experience and U.S. investigation device exemption study,” *Spine*, vol. 28, no. 20, pp. S163-166, Oct. 2003.

[12] M. Putzier *et al.*, “Charité total disc replacement—clinical and radiographical results after an average follow-up of 17 years,” *Eur. Spine J.*, vol. 15, no. 2, pp. 183–195, Feb. 2006.

[13] B. J. C. Freeman and J. Davenport, “Total disc replacement in the lumbar spine: a systematic review of the literature,” *Eur. Spine J.*, vol. 15, no. Suppl 3, pp. 439–447, Aug. 2006.

[14] L. Jackson, D. R. Jones, P. Scotting, and V. Sottile, “Adult mesenchymal stem cells: Differentiation potential and therapeutic applications,” *J. Postgrad. Med.*, vol. 53, no. 2, p. 121, Jan. 2007.

[15] L. Orozco, R. Soler, C. Morera, M. Alberca, A. Sánchez, and J. García-Sancho, “Intervertebral disc repair by autologous mesenchymal bone marrow cells: a pilot study,” *Transplantation*, vol. 92, no. 7, pp. 822–828, Oct. 2011.

[16] G. Vadalà, G. Sowa, M. Hubert, L. G. Gilbertson, V. Denaro, and J. D. Kang, “Mesenchymal stem cells injection in degenerated intervertebral disc: cell leakage may induce osteophyte formation,” *J. Tissue Eng. Regen. Med.*, vol. 6, no. 5, pp. 348–355, May 2012.

[17] C. G. Pfeifer *et al.*, "Higher Ratios of Hyaluronic Acid Enhance Chondrogenic Differentiation of Human MSCs in a Hyaluronic Acid–Gelatin Composite Scaffold," *Materials*, vol. 9, no. 5, May 2016.

[18] C. B. Knudson and W. Knudson, "Cartilage proteoglycans," *Semin. Cell Dev. Biol.*, vol. 12, no. 2, pp. 69–78, Apr. 2001.

[19] C. E. Schanté, G. Zuber, C. Herlin, and T. F. Vandamme, "Chemical modifications of hyaluronic acid for the synthesis of derivatives for a broad range of biomedical applications," *Carbohydr. Polym.*, vol. 85, no. 3, pp. 469–489, Jun. 2011.

[20] J. Seon Kwon *et al.*, "Injectable in situ -forming hydrogel for cartilage tissue engineering," *J. Mater. Chem. B*, vol. 1, no. 26, pp. 3314–3321, 2013.

[21] Tan Wei, Vinegoni Claudio, Norman James J., Desai Tejal A., and Boppart Stephen A., "Imaging cellular responses to mechanical stimuli within three-dimensional tissue constructs," *Microsc. Res. Tech.*, vol. 70, no. 4, pp. 361–371, Jan. 2007.

[22] R. Galli *et al.*, "Raman-based imaging uncovers the effects of alginate hydrogel implants in spinal cord injury," in *Advanced Microscopy Techniques IV; and Neurophotonics II*, 2015, vol. 9536, p. 95360Y.

[23] Y. Liang, A. Bar-Shir, X. Song, A. A. Gilad, P. Walczak, and J. W. M. Bulte, "Label-Free Imaging of Gelatin-Containing Hydrogel Scaffolds," *Biomaterials*, vol. 42, pp. 144–150, Feb. 2015.

[24] J. H. Ardenkjær-Larsen *et al.*, "Increase in signal-to-noise ratio of > 10,000 times in liquid-state NMR," *Proc. Natl. Acad. Sci.*, vol. 100, no. 18, pp. 10158–10163, Sep. 2003.

[25] M. Srinivas, A. Heerschap, E. T. Ahrens, C. G. Figdor, and I. J. M. de Vries, "19F MRI for quantitative in vivo cell tracking," *Trends Biotechnol.*, vol. 28, no. 7, pp. 363–370, Jul. 2010.

[26] C. Constantinides *et al.*, "Fast, quantitative, murine cardiac 19F MRI/MRS of PFCE-labeled progenitor stem cells and macrophages at 9.4T," *PLOS ONE*, vol. 13, no. 1, p. e0190558, Jan. 2018.

[27] U. Flögel *et al.*, "In vivo monitoring of inflammation after cardiac and cerebral ischemia by fluorine magnetic resonance imaging," *Circulation*, vol. 118, no. 2, pp. 140–148, Jul. 2008.

[28] E. T. Ahrens and J. Zhong, "In vivo MRI cell tracking using perfluorocarbon probes and fluorine-19 detection," *NMR Biomed.*, vol. 26, no. 7, pp. 860–871, Jul. 2013.

[29] M. S. Fox, J. M. Gaudet, and P. J. Foster, "Fluorine-19 MRI Contrast Agents for Cell Tracking and Lung Imaging," *Magn. Reson. Insights*, vol. 8, no. Suppl 1, pp. 53–67, Mar. 2016.

[30] G. M. Lanza *et al.*, "Targeted Antiproliferative Drug Delivery to Vascular Smooth Muscle Cells With a Magnetic Resonance Imaging Nanoparticle Contrast Agent: Implications for Rational Therapy of Restenosis," *Circulation*, vol. 106, no. 22, pp. 2842–2847, Nov. 2002.

[31] T. Lammers *et al.*, "Fluorinated polyurethane scaffolds for 19F magnetic resonance imaging," *Chem. Mater. Publ. Am. Chem. Soc.*, vol. 29, no. 7, pp. 2669–2671, Apr. 2017.

[32] D. Pan, G. M. Lanza, S. A. Wickline, and S. D. Caruthers, "Nanomedicine: Perspective and promises with ligand-directed molecular imaging," *Eur. J. Radiol.*, vol. 70, no. 2, pp. 274–285, May 2009.

[33] G. Marshall and C. Kasap, “Adverse events caused by MRI contrast agents: Implications for radiographers who inject,” *Radiography*, vol. 18, no. 2, pp. 132–136, May 2012.

[34] K. Waxman, “Perfluorocarbons as blood substitutes,” *Ann. Emerg. Med.*, vol. 15, no. 12, pp. 1423–1424, Dec. 1986.

[35] A. H. Schmieder, S. D. Caruthers, J. Keupp, S. A. Wickline, and G. M. Lanza, “Recent Advances in 19Fluorine Magnetic Resonance Imaging with Perfluorocarbon Emulsions,” *Engineering*, vol. 1, no. 4, pp. 475–489, Dec. 2015.

[36] S. Waiczies *et al.*, “Enhanced Fluorine-19 MRI Sensitivity using a Cryogenic Radiofrequency Probe: Technical Developments and Ex Vivo Demonstration in a Mouse Model of Neuroinflammation,” *Sci. Rep.*, vol. 7, no. 1, Dec. 2017.

[37] Z. Z. Zheng *et al.*, “Incorporation of quantum dots in silk biomaterials for fluorescence imaging,” *J. Mater. Chem. B Mater. Biol. Med.*, vol. 3, no. 31, pp. 6509–6519, Aug. 2015.

[38] X. Cheng, J. Liu, L. Wang, R. Wang, Z. Liu, and R. Zhuo, “An enzyme-mediated in situ hydrogel based on polyaspartamide derivatives for localized drug delivery and 3D scaffolds,” *RSC Adv.*, vol. 6, no. 103, pp. 101334–101346, 2016.

[39] Inserm U1026, Université Bordeaux Segalen, F-33076 Bordeaux, France *et al.*, “Magnetic resonance imaging tracking of human adipose derived stromal cells within three-dimensional scaffolds for bone tissue engineering,” *Eur. Cell. Mater.*, vol. 21, pp. 341–354, Apr. 2011.

[40] L. Cao, B. Cao, C. Lu, G. Wang, L. Yu, and J. Ding, “An injectable hydrogel formed by in situ cross-linking of glycol chitosan and multi-benzaldehyde functionalized

PEG analogues for cartilage tissue engineering," *J. Mater. Chem. B*, vol. 3, no. 7, pp. 1268–1280, 2015.

[41] R. Battino, T. R. Rettich, and T. Tominaga, "The Solubility of Nitrogen and Air in Liquids," *J. Phys. Chem. Ref. Data*, vol. 13, no. 2, pp. 563–600, Apr. 1984.

[42] W. D. Mcelroy, H. H. Seliger, and E. H. White, "MECHANISM OF BIOLUMINESCENCE, CHEMI-LUMINESCENCE AND ENZYME FUNCTION IN THE OXIDATION OF FIREFLY LUCIFERIN*,†," *Photochem. Photobiol.*, vol. 10, no. 3, pp. 153–170, Sep. 1969.

Curriculum Vitae

Shinnosuke (Shin) Fukazawa
sfukaza1@jhu.edu | Baltimore, MD 21218

Education

Johns Hopkins University
M.S.E. in Biomedical Engineering - May 2018 (expected)

University of California, Irvine
B.S. in Biomedical Engineering -2016
-Specialization in Bio-photonics & Minor in Material Science Engineering
Cum Laude

Research Experience

Johns Hopkins Depart. of Radiology and Radiological Sciences - 2016~2018
• Research in potential imaging agents for monitoring hydrogels intended for application in transplanting stem cells in regenerative therapy.
• Research planning and journal writing, as well as technical skills in cell culturing, tissue scaffold developing, and Magnetic Resonance Imaging (MRI) were developed.

Laboratory for Fluorescence Dynamics (Senior Project) - 2015~2016
• Worked in a team to design a prototype of an embryo viability assessment device for in vitro fertilization utilizing laser imaging of embryos.
• Also worked on the business aspect and generated funds for development of the device through pitches/business competitions.

Beckman Laser Institute - 2014~2016
• Researched effects of photothermal damage in mice vasculature utilizing laser speckle imaging.

Honors & Awards /Honor Society

Paul Merage Business Plan Competition 2016
• Pitched the prototype device aforementioned to investors and faculty and won 1st place in 2 tracks; obtained $30,000 in monetary awards.

Summer Undergraduate Research Program – 2015: $1500 award
Undergraduate Research Opportunity Program – 2015: $1300 award

Tau Beta Pi
Alpha Eta Mu Beta - 2013~2016
• Mentorship for peer biomedical engineers and improved curriculum through consultation with professors.